4600

ARMY RESEARCH LABORATORY

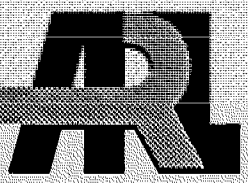

A Uniaxial Nonlinear Viscoelastic Constitutive Model With Damage for M30 Gun Propellant

George A. Gazonas

ARL-TR-115

April 1993

REPORT DOCUMENTATION PAGE

Form Approved
OMB No. 0704-0188

1. AGENCY USE ONLY *(Leave blank)*	2. REPORT DATE	3. REPORT TYPE AND DATES COVERED
	April 1993	Final- Sep 91 - Jul 92

4. TITLE AND SUBTITLE
A Uniaxial Nonlinear Viscoelastic Constitutive Model with Damage for M30 Gun Propellant

5. FUNDING NUMBERS
PR: 1L161102AH43

6. AUTHOR(S)
George A. Gazonas

7. PERFORMING ORGANIZATION NAME(S) AND ADDRESS(ES)
U.S. Army Research Laboratory
ATTN: AMSRL-WT-PE
Aberdeen Proving Ground, MD 21005-5066

8. PERFORMING ORGANIZATION REPORT NUMBER

9. SPONSORING/MONITORING AGENCY NAMES(S) AND ADDRESS(ES)
US Army Research Laboratory
ATTN: AMSRL-OP-CI-B (Tech Lib)
Aberdeen Proving Ground, MD 21005-5066

10. SPONSORING/MONITORING AGENCY REPORT NUMBER
ARL-TR-115

11. SUPPLEMENTARY NOTES

12a. DISTRIBUTION/AVAILABILITY STATEMENT
Approved for public release; distribution is unlimited.

12b. DISTRIBUTION CODE

13. ABSTRACT *(Maximum 200 words)*

The nonlinear viscoelastic mechanical response of a conventional tank gun propellant, M30, is modeled using a "modified superposition integral" which incorporates the effects of microstructural fracture damage. Specifically, a linear, time-dependent kernel is convolved with the first-time derivative of a power-law function of stress and a damage "softening" function which accounts for damage evolution by a microcrack growth mechanism. The microcrack damage function is a master curve formed from shifted isothermal, compressive, uniaxial constant strain rate (.01 1/s to 420 1/s) data on solid, right-circular cylinders of M30 gun propellant. An attractive feature of the model is its ability to predict work-softening behavior under conditions of monotonically increasing deformation. Time-dependent predictions of stress versus time, failure stress versus failure time, and failure stress versus strain rate, quantitatively agree with experimental results from constant strain rate tests on the propellant. Theoretical predictions of time-dependent stresses for Heaviside and "ballistic-like" strain histories are also provided.

14. SUBJECT TERMS
constitutive modeling, M30 gun propellant, continuum damage mechanics, nonlinear viscoelasticity, uniaxial compression testing, viscoelasticity, continuum mechanics

15. NUMBER OF PAGES
36

16. PRICE CODE

17. SECURITY CLASSIFICATION OF REPORT	18. SECURITY CLASSIFICATION OF THIS PAGE	19. SECURITY CLASSIFICATION OF ABSTRACT	20. LIMITATION OF ABSTRACT
UNCLASSIFIED	UNCLASSIFIED	UNCLASSIFIED	SAR

INTENTIONALLY LEFT BLANK.

TABLE OF CONTENTS

INTENTIONALLY LEFT BLANK.

LIST OF FIGURES

LIST OF TABLES

INTENTIONALLY LEFT BLANK.

1. INTRODUCTION

The uniaxial compressive mechanical response of M30 gun propellant is well documented over the temperature range from -40 to 60 degrees Celsius, and strain rates from quasistatic to 10^4 sec^{-1} using drop weight (Lieb 1989), split Hopkinson bar (Lieb et al 1989), and servohydraulic (Gazonas 1991; Gazonas and Ford 1992) test apparatuses. Uniaxial compression of right-circular cylinders of M30 induces fracture damage consisting of axial cracks that grow and eventually coalesce to form macroscopic conjugate shear fractures at large strains. Micrographic evidence reveals that microcracks initially form between the subaxially oriented nitroguanidine crystallites (energetic filler) and the nitrocellulose (binder). The stress-strain response of M30 is slightly nonlinear prior to the maximum stress level (failure stress); the propellant subsequently work-softens until ultimate failure or rupture occurs (Gazonas and Ford 1992).

Despite the large body of work that documents the mechanical properties of gun propellants, studies related to their constitutive characterization are scarce. A recent study characterizes the viscoelastic response of M30 propellant and shows that the propellant exhibits nonlinear (strain-dependent) power-law relaxation over the time interval 10^{-2} to 10^{+4} milliseconds (Gazonas 1991). A complete constitutive description of the solid propellant phase is critical for accurate description of combustion in numerical models (Gough 1990) of the interior ballistic (IB) process because the rate of mass generation of the gaseous phase during combustion is proportional to the amount of exposed propellant surface area (see Military Explosives 1955). Early models of combustion assume that time-dependent surface area is only a function of the differential changes in the initial propellant geometry caused by deflagration. These models do not account for an increase in surface area due to deformation and fracture of the propellant. Subsequent IB numerical models incorporate the effect of enhanced mass generation rate due to fracture by using surface area "multipliers" (Keller and Horst 1989). It is anticipated that the constitutive and damage characterization of single-grains

of propellant will provide insight into the physics governing the bulk deformation of granular propellant beds.

This paper employs a uniaxial specialization of a general three-dimensional constitutive theory for viscoelastic materials with damage (Schapery 1981). Several features of the constitutive theory make it an attractive candidate for modeling the constitutive behavior of M30 propellant. First, the theory can predict the observed work-softening behavior in M30 under monotonically increasing deformation. Microcracking materials that exhibit work-softening behavior pose special problems for constitutive modelers since it can be argued that "shear" fracture planes that develop in many materials in compression are structural or geometric features that corrupt detection of the true material response of the material as it work-softens. Additional problems associated with a loss of hyperbolicity of the wave equation in damaged, work-softening materials have recently been addressed using a nonlocal elasticity approach (Valanis 1991). Secondly, the constitutive equations can be transformed to those of nonlinear elastic materials through correspondence principles. The transformation facilitates the solution of boundary value problems encountered in the theory of nonlinear viscoelasticity. Thirdly, microcracking in M30 is characterized with a damage function that is related to time-dependent surface area evolution in the propellant. This relation could be incorporated into IB numerical codes for more accurate prediction of surface area evolution and mass generation rate during propellant combustion. Finally, the theory is general enough to successfully describe the nonlinear viscoelastic response of a variety of other materials that include: marine sediment (Schapery and Riggins 1982), rocket propellant (Schapery 1982), and ice (Harper 1986; Harper 1989). Thus, material constitution and damage evolution in a variety of materials can be compared within the framework of a single theory.

Even though "material" damage is treated herein as a scalar-valued quantity, predictions of stress versus time, failure stress versus failure time, and failure stress versus strain rate quantitatively agree with observations from isothermal, uniaxial, constant strain rate compression tests on the propellant. It is shown that microcracking in M30 is characterized by an "ellipsoidal" damage

function, formed from shifted isothermal constant strain rate test data. The form of the "ellipsoidal" damage function is compared with damage functions that have been developed for other materials such as, ice in compression (Harper 1986), and oil-shale under dynamic blast conditions (Grady and Kipp 1980).

2. THE CONSTITUTIVE THEORY

The uniaxial nonlinear viscoelastic constitutive equation for materials that possess a random or regular distribution of microcracks can be written with a so-called "modified superposition integral" (Schapery 1981; Schapery 1989). The uniaxial strain ε in a material subjected to a uniaxial stress σ can be written as

$$\varepsilon(t) = E_r \int_0^t D(t - \tau) \frac{df}{d\tau} d\tau \quad , \qquad (1)$$

The integral in (1) is also known as an hereditary integral or as a convolution of the functions D and $\dot{f}$. Material nonlinearities and damage are usually incorporated in the function f, where

$$f = f(\sigma, S_{\sigma k}) \quad . \qquad (2)$$

In (1), E_r is an arbitrary constant referred to as the "reference" modulus with units of stress. Elastic behavior is obtained when $D = E_r^{-1}$. D(t) is the linear viscoelastic creep compliance if all material nonlinearities are incorporated into f. The creep compliance is defined as the strain response normalized to the unit stress input (i.e., $D(t) = \varepsilon(t)/\sigma_o$, with $\sigma(t) = \sigma_o H(t)$, and $H(\zeta)$ is the Heaviside function defined as, $H(\zeta) = 1$ for $\zeta > 0$, and $H(\zeta) = 0$ for $\zeta < 0$). In (2), the $S_{\sigma k}$ are k, time-dependent damage parameters that influence the time-dependent strain in (1). The σ-subscript in (2) refers to damage parameters developed for stress-history inputs. The damage parameters $S_{\varepsilon k}$ are used for strain-history inputs. In (2), f is written in product form with a power-law stress function g_1 and a

damage function $g_{2\sigma}$ as

$$f = g_1(\sigma)\, g_{2\sigma}(S_\sigma) = \left(\frac{\sigma}{\sigma_2}\right)^r e^{\lambda S_\sigma} \operatorname{sgn}(\sigma) \quad . \tag{3}$$

where σ_2, r and λ are positive constants. The stress-history dependent damage parameter is derived (Schapery 1981) by integrating the relation between crack-tip velocity and the J-integral and is given by

$$S_\sigma = \int_0^t \left|\frac{\sigma}{\sigma_1}\right|^q f_1 \, dt \quad , \tag{4}$$

where σ_1 and q are positive constants, and | | denotes the absolute value of the quantity. A damage parameter similar to (4) is derived by Wnuk and Kriz (1985) by integration of the "Kachanov" equation which relates the rate of damage growth to a power-law function of the net-section stress. The functions g_1 and $g_{2\sigma}$, and the above constants may be different for characterizing material behavior in compression versus tension or for unloading after significant plasticity. The general validity of the theory can be verified if the above constants and functions, g_1 and $g_{2\sigma}$, are unique for a variety of stress-history inputs in (1). The signum function in (3) is defined as $\operatorname{sgn}(\sigma) = 1$ for compression in this study. f_1 is a "crack-tip material coefficient" which can depend on time and temperature and material aging effects (Schapery 1981). In the present study $f_1 = 1$. The damage function $g_{2\sigma}(S_\sigma)$ in (3) reflects material damage due to microcracks. The exponential form of $g_{2\sigma}$ was originally proposed by Schapery (1981) and was later used to model microstructural damage in ice subjected to uniaxial compression (Harper 1986). Later, it is shown that the exponential damage function which characterizes damage in ice does not satisfactorily characterize damage in M30 propellant. Instead, an "ellipsoidal" damage function is utilized that is directly determined from the test data. From (3) we see that in the absence of damage, $S_\sigma = 0$ and $g_{2\sigma} = 1$, and (1) then predicts strain in a nonlinear viscoelastic material without damage. Material symmetry changes due to damage induced anisotropy are not addressed in this paper and damage is treated as a scalar-valued quantity. More discus-

sion of this topic and higher-order tensorial descriptions of damage can be found in the papers of Krajcinovic (1987) and Weitsman (1988).

Equations (1) through (4) are suitable for characterizing damage and a material's strain response if stress is a controlled input for the test. However, if strain is a controlled input for the test, then these equations must be inverted in order to predict stress as a function of strain history

$$\sigma(t) = \sigma_2 \, \varepsilon^{o\,1/r} \, g_{2\varepsilon}(S_\varepsilon) \, \mathrm{sgn}(\varepsilon^o) \quad , \tag{5}$$

where $g_{2\varepsilon}(S_\varepsilon) = g_{2\sigma}(S_\sigma)^{-1/r}$, and the pseudo-strain ε^o is related to strain history by

$$\varepsilon^o = E_r^{-1} \int_0^t E(t-\tau) \frac{d\varepsilon}{d\tau} \, d\tau \quad . \tag{6}$$

where E(t) is the relaxation modulus. Schapery (1982) points out that the utility of pseudo-strain, as a strain measure, lies in that fact that stress versus pseudo-strain plots are single-valued or "elastic-like" for cyclically-strained materials. However, the $\varepsilon \rightarrow \varepsilon^o$ transformation in (6) does not produce a single-valued curve for materials that work-soften. The damage parameter S_ε is obtained by substitution of (5) into the time-derivative of (4). Rearrangement and integration of the result leads to

$$S_\varepsilon = \int_0^{S_\sigma} g_{2\sigma}(S_\sigma)^{q/r} \, dS_\sigma \quad , \tag{7}$$

or

$$S_\varepsilon = (\sigma_2/\sigma_1)^q \int_0^t \varepsilon^{o\,q/r} f_1 \, dt \quad . \tag{8}$$

The lower limit in (7) is zero, which corresponds to a no-damage condition at time t = 0. If an exponential form $g_{2\sigma}(S_\sigma) = e^{\lambda S\sigma}$ is used in (7), then the damage function becomes

$$g_{2\varepsilon}(S_\varepsilon) = (1 + \lambda q S_\varepsilon / r)^{-1/q} \quad . \tag{9}$$

The derivation of a more general damage function is obtained if one assumes a product form for f as given by (3). Substitution of the first time-derivative of (4) into that of (3) results in a nonlinear differential equation (Bernoulli equation), solvable for stress, which can be linearized and integrated using a power-law function of the pseudo-strain as an integrating factor (Appendix). The identity,

$$f = \varepsilon^{\circ} \quad , \tag{10}$$

is used in the derivation and is obtained if $\tilde{E}\ \tilde{D} = 1$, where $\tilde{E}$ and $\tilde{D}$ are the Carson transformed relaxation modulus and creep compliance respectively. A generalized form of the damage function is then given as

$$g_{2\varepsilon}(S_\varepsilon) = (1 + qS_\varepsilon/r)^{-1/q} \quad . \tag{11}$$

and the generalized damage parameter is

$$S_\varepsilon = (\sigma_2/\sigma_1)^q \int_0^t \varepsilon^{\circ q/r} \frac{dg_{2\sigma}}{dS_\sigma} \frac{f_1}{g_{2\sigma}}\, dt \quad . \tag{12}$$

If $g_{2\sigma}(S_\sigma) = e^{\lambda S\sigma}$ in (12), then $dg_{2\sigma}/dS_\sigma\ g_{2\sigma}^{-1} = \lambda$, and the more general (11) reduces to (9).

2.1. Predictions for Constant Strain-Rate Compression Tests. This section provides expressions for predicting stress and damage functions for constant strain rate tests. For a constant strain rate $\dot{\varepsilon}$ input,

$$\varepsilon(t) = \dot{\varepsilon}\, t\, H(t) \quad . \tag{13}$$

Substitution of (13) into (6) with the power-law relaxation modulus of M30 determined earlier (Gazonas 1991), $E(t) = E_1 t^n$, (typically $0 < n < 1$), and $E_1 = E_r$, yields the pseudo-strain

$$\varepsilon^{o}(t) = \dot{\varepsilon}\, t^{(1-n)}/(1-n) \tag{14}$$

and for the damage parameter,

$$S_\varepsilon(t) = \left(\frac{\dot{\varepsilon}}{\dot{\varepsilon}_{ref}}\frac{1}{(1-n)}\right)^{q/r} \frac{t^{\alpha}}{\alpha} \quad , \tag{15}$$

where $\alpha = (1-n)q/r + 1$. The constant σ_1 is replaced by the reference strain rate, $\dot{\varepsilon}_{ref}$, with the relation $\sigma_1 = \sigma_2\, \dot{\varepsilon}_{ref}^{1/r}$. Substitution of (14) into (5) provides the time-dependent stress

$$\sigma(t) = \sigma_2 \left(\frac{\dot{\varepsilon}\, t^{(1-n)}}{1-n}\right)^{1/r} g_{2\varepsilon}(S_\varepsilon)\ \mathrm{sgn}(\varepsilon^{o}) \quad , \tag{16}$$

where $\mathrm{sgn}(\varepsilon^{o}) = 1$ for monotonically increasing functions ε^{o}.

3. EXPERIMENTAL RESULTS

Experimental results for isothermal uniaxial compression of M30 at four strain rates appear in Figure 1. Each stress-time curve is a composite curve formed from the average of five tests. The compression tests are performed utilizing a servohydraulic test apparatus (MTS 810 High Rate Test System) that is described in more detail elsewhere (Gazonas 1991). The maximum piston velocity is on the order of 12 meters/sec (39.4 feet/sec) (and this limits the axial compressive strain rate to 500 sec^{-1} in 25.4 mm (1 inch) long specimens. Constant strain rate tests are performed by computer control of the piston velocity via feedback from an externally mounted transducer, linear-variable differential transformer (LVDT), MTS Model 244.11. Force is measured with a 60 kN (13.5×10^3

lb), quartz-piezoelectric force transducer, Kistler Type 9031A, which is mounted on the upper moving piston. Specimen displacements are corrected for apparatus distortion which has a measured stiffness of about 91.9 kN/mm (52.4 x 10^4 lb/in). Specimen stiffness ranges from 4.5 to 14.0 kN/mm over the strain rates investigated. Tests are conducted at a room temperature of 22 ± 1 degrees Celsius.

Right-circular cylinders of M30 gun propellant (Radford lot # 128 B) are prepared by cutting specimens from six-inch, solid, stick propellant using an Isomet, double-bladed diamond saw. The inert lubricant, molybdenum disulfide, MoS_2, is sparingly applied to the specimen ends to reduce end friction effects and test variability (Gazonas and Ford 1992). The chemical composition and nominal specimen dimensions of M30 appear in Table 1.

4. DETERMINATION OF MODEL PARAMETERS

Constitutive response predictions from the nonlinear theory described above are made by first determining constants, σ_2, n, r, $\dot{\varepsilon}_{ref}$, and q, and the damage function $g_{2\varepsilon}$ in (14) through (16). The material constants are determined from a limited set of experimental data (constant strain rate tests) for prediction of material response under more general input histories.

The damage function and constants are obtained by plotting $\log_{10} g_{2\varepsilon}(S_\varepsilon)$ in (16) versus $\log_{10} S_\varepsilon$ in (15). Experimental $\sigma(t)$ data are used in (16). Damage curves for a set of arbitrarily chosen constants, σ_2, r, n, and q, appear in Figure 2. However, if two curves, taken at the strain rate extremes (.01 sec^{-1} and 420 sec^{-1}) are shifted, a "master" damage function is formed with an appropriate choice of constants (determined by trial-and-error, see Figure 3a) which are: σ_2 = 670 MPa (97.2 x 10^6 psi), r = 1.2, n = 0.1, q = 9, and $\dot{\varepsilon}_{ref}$ = .01 sec^{-1}. The master damage function takes an "ellipsoidal" form (solid line in Figure 3b) in logarithmic coordinates and represents the "softening" effect of the microcracks;

$$\mathrm{Log}_{10}\, g_{2\varepsilon}(S_\varepsilon) = -1.5\,(1 - \sqrt{1-\xi^2}) \quad , \tag{17}$$

where $\xi = \log_{10}(S_\varepsilon) / \log_{10}(S_{\varepsilon max})$

and the microcrack "saturation" level is at $\log_{10}(S_{\varepsilon max}) = 10$.

5. DAMAGE FUNCTION COMPARISON TO OTHER FORMS

The damage function developed herein for M30 propellant is compared to damage functions used for describing microcrack growth in ice in compression (Harper 1986) and dynamic blast and fragmentation of oil-shale (Grady and Kipp 1980) (Figure 4a). The damage function for ice is based on an exponential form and is unsuitable for M30 propellant since the slope of the function $g_{2\varepsilon}(S_\varepsilon)$ in logarithmic coordinates is linear and proportional to -1/q (see (9)) whereas experimental data for M30 in these coordinates are nonlinear (Figure 3a). The damage function for dynamic fragmentation of oil-shale,

$$g_{2\varepsilon} = 1 - D = 1 - a\dot{\varepsilon}^{m} t^{m+3} \quad , \tag{18}$$

is microstructurally derived from a two-parameter Weibull crack distribution function (Grady and Kipp 1980) and has been successfully used to predict fragment size and the fracture stress dependence on strain rate

$$\sigma(t) = B\dot{\varepsilon}\, t\,(1 - D) \quad , \tag{19}$$

Damage is defined here as a scalar quantity, $0 < D < 1$, and $D = 0$ corresponds to a no-damage condition, whereas $D = 1$ corresponds to complete material failure. In (18), a and m are constants, and in (19), $\dot{\varepsilon}$ is the strain rate, t is time, and B is the intrinsic elastic modulus. Numerical values

for the constants used to plot (9) and (18) in Figure 4a can be found in the original references (Harper 1986; Grady and Kipp 1980). The ultimate utility of the damage function lies in its ability to accurately model material behavior, regardless of the method used in its determination. However, models developed from microstructural considerations are intrinsically more appealing than those developed from empirical data fits.

5.1 Significance of Parameter D: Fracture Surface Area. A number of authors have attributed microstructural significance to D which is assumed to be proportional to: 1) the ratio of the microcrack area to total area, A_c/A, (Schapery 1981; Lemaitre 1985), 2) ratio of defect density to a "saturation" defect density, d/d_s, (Rousselier 1981), 3) the ratio of the radius of a single spherical microcrack to the volume of a representative unit cell, a^3/V, (Budiansky and O'Connell 1976), and 4) statistical distributions of the ratio of the number of broken bonds in "bundle" models to the total number of bonds, n/N, (Bolotin 1969), to name a few. For reasons of relative simplicity, most microstructural models are developed for cracks which grow normal to an applied tensile stress field. For materials in compression, mixed mode crack growth and interaction considerably complicates both the development of microstructural models and the functional relation between crack speed and stress intensity factor (Costin 1987). It is not the intent of this study to develop a microstructural model for microcrack growth in M30 in compression. However, D could be expressed in terms of the ratio of microcrack area to the "saturation" microcrack area, A_c/A_s, (motivated by the form of g_{2e} in (17)). Figure 4b compares D vs Log_{10} Time for M30, ice, and oil-shale. The time-rate of change of D increases with strain rate, i.e. $dD/dt = f(\dot{\varepsilon})$.

Observations indicate that the amount of damage (fracture surface-area) in M30 propellant is relatively insensitive to strain rate from 10^{-2} sec^{-1} to 100 sec^{-1}. Over this strain rate range, fracture surface-area production is primarily dependent on the amount of axial specimen strain (i.e. D = g(e)) and secondarily dependent on the deformation temperature (Gazonas et al 1991). However,

theoretical predictions of fragment size in oil-shale subjected to dynamic loading indicate that fragment size decreases as strain rate increases (Grady and Kipp 1980). Furthermore, fragment size in oil-shale decreases from 0.1 to .01 meters as strain rate increases in the moderate loading rate regime from 10 sec^{-1} to 100 sec^{-1}. The damage function and material constants determined in this study may not appropriately model the constitutive response of M30 propellant under more dynamic loading conditions. Additional material data obtained at large, dynamic strain rates are needed to accurately predict material behavior over the wide spectrum of strains and loading rates experienced by the propellant in the gun during firing. The next section compares data and constitutive predictions of time-dependent stresses in M30 in order to verify the theory and illustrate its general utility.

6. CONSTANT STRAIN-RATE COMPRESSION

Time-dependent stresses for constant strain rate deformation of M30 are predicted by solving (17) for $g_{2\varepsilon}(S_\varepsilon)$ and substituting the result into (16). Stress versus time predictions are plotted in Figure 5 (solid lines) for the strain rate extremes at which the damage function is defined. Experimental data (symbols) are also plotted for comparison with the theoretical predictions. Superposed curves at intermediate strain rates (0.9 sec^{-1} and 89 sec^{-1}) reflect the predictive capability of the theory since $g_{2\varepsilon}(S_\varepsilon)$ is determined from data shifted from the strain rate extremes. The theoretical expression in (16) provides a good approximation to actual stress-time data obtained at constant strain rate. A cursory inspection of the superimposed stress versus time curves reveals that the theory accurately predicts maximum or "failure" stresses, failure times, and the work-softening characteristics of M30 propellant. A closed-form expression for the failure time (time at maximum stress level) is obtained by setting the stress-rate in (5) equal to zero, ($d\sigma/dt = 0$) i.e.,

$$\frac{d\sigma}{dt} = \varepsilon^{o\,1/r}\,\frac{d(g_{2\varepsilon})}{dt} + g_{2\varepsilon}\,\frac{d(\varepsilon^{o\,1/r})}{dt} = 0 \qquad (20)$$

Using the chain rule of differentiation for the first term in (20), $d(g_{2\varepsilon})/dt = d(g_{2\varepsilon})/dS_\varepsilon \; dS_\varepsilon/dt$, and after some algebraic manipulation, the principal result is that at the maximum stress, $\xi_f = \xi$ at failure = constant, i.e.,

$$\xi_f = \sqrt{\frac{1}{\beta^2 + 1}} = 0.542 \quad , \qquad (21)$$

where $\beta = 1.5\, \alpha\, r /(\log_{10}(S_{\varepsilon max})\,(1-n))$. Since $\xi = \log_{10}(S_\varepsilon) / \log_{10}(S_{\varepsilon max})$, the damage parameter at the failure stress is constant, i.e., $S_\varepsilon(\xi_f) = 10^{5.42}$. The time required to reach maximum stress, or failure time, is determined by solving (15) for t_f subject to condition (21),

$$t_f = (S_\varepsilon(\xi_f)\;\; (\dot{\varepsilon}\,/(1-n)\,\dot{\varepsilon}_{ref}^{\,-q/r}\,\alpha)^{1/\alpha} \quad . \qquad (22)$$

The failure stress is obtained by substitution of (22) into (16) to obtain

$$\sigma(t_f) = \sigma_2\; \overset{o}{\varepsilon}_f^{\,1/r}(t_f)\; g_{2\varepsilon}(\xi_f) \quad . \qquad (23)$$

The log failure stress versus log failure time is plotted in Figure 6. The predictions (solid symbols) compare well with observed failure stresses and observed failure times (open symbols). The failure stress is also observed to monotonically increase with strain rate (open symbols in Figure 7). The monotonic increase in failure stress with strain rate is also predicted by (23) (solid symbols) and the weak strain rate dependence is given by $\sigma_f = 59\; \dot{\varepsilon}^{\,0.093}$. The failure stress is insensitive to strain rate if $n << 1$ in (22) and (23). The theory predicts that the strain at failure,

$$\varepsilon_f = t_f \dot{\varepsilon} \quad , \qquad (24)$$

is independent of strain rate in materials if r = nq (Harper 1986). This result is deduced by substituting (22) into (24) with r = nq. The strain rate independence of failure strain is also predicted by the theory in materials if r = 1 and n << 1, as in linear elastic materials with damage. Both constraint conditions are approximately true for M30 material constants, and this may explain why measured yield strains (approximately equal to failure strains) in M30 are insensitive to strain rate (Gazonas 1991; Gazonas and Ford 1992). In addition to being strain rate independent, the failure strain is seen to take on a constant value since the slope of failure stress versus failure time curve (Figure 6) and the slope failure stress versus strain rate curve (Figure 7) are equal in magnitude, but opposite in sign.

6.1 More Complex Input Histories. Closed-form analytical expressions for time-dependent stresses are determined if the product of the relaxation modulus and the strain history in (6) is an integrable function. Strain histories of arbitrary complexity can be approximated using a large number of constant strain rate ramp functions. As an illustration, an input history that consists of two, successive, constant strain rate ramps is expressed by

$$\varepsilon(t) = \dot{\varepsilon}_1 \, t \, H(t) + (\dot{\varepsilon}_2 - \dot{\varepsilon}_1) \, t \, H(t - t_1) \quad , \tag{25}$$

where $\dot{\varepsilon}_1$ and $\dot{\varepsilon}_2$ are the constant strain rates of each ramp and t_1 is the time of application of strain rate $\dot{\varepsilon}_2$. Time-dependent stresses are determined by substituting (25) into (6). Two examples that illustrate such ramp inputs include: 1) time-dependent stress predictions for stress-relaxation of M30 after a period of constant strain rate straining appears in Figure 8, and 2) a "ballistic-like" input, simulated by a concave-up, two-ramp, input history, with the strain rate in the second ramp an order of magnitude greater than the strain rate in the first ramp (Figure 9). A comparison of the constitutive response of M30 under a variety of input histories, such as those given in this section, will provide a more general verification of the theory. Experimental programs should include input histories that are similar to those experienced by the propellant in the gun during firing.

7. CONCLUDING REMARKS

A nonlinear theory of viscoelasticity with damage has been shown to accurately model the constitutive response of M30 gun propellant in uniaxial, isothermal compression. The exponential damage function $e^{\lambda S\sigma}$ originally proposed by Schapery (1981) and used to describe uniaxial deformation and failure in ice (Harper 1986) was found unsuitable for describing deformation and failure in M30 propellant. Instead, an "ellipsoidal" damage function was determined, directly from the data, which accurately predicted worksoftening behavior under monotonically increasing deformation. In addition, time-dependent predictions of stress versus time, and failure stress versus failure time, and failure stress versus strain rate, quantitatively agree with experimental results from constant strain rate tests on the propellant. The observed insensitivity of failure strains to strain rate in M30 (Gazonas 1991; Gazonas and Ford 1992) is a result that is also derivable from the theory. Future work is planned to verify the generality of the constitutive model under more complex input histories such as those described in the previous section. However, significant plastic deformation that is observed in the propellant after unloading may pose difficulties for the model. An extension of the model to include temperature-dependent behavior with reduced time variables is also currently under development.

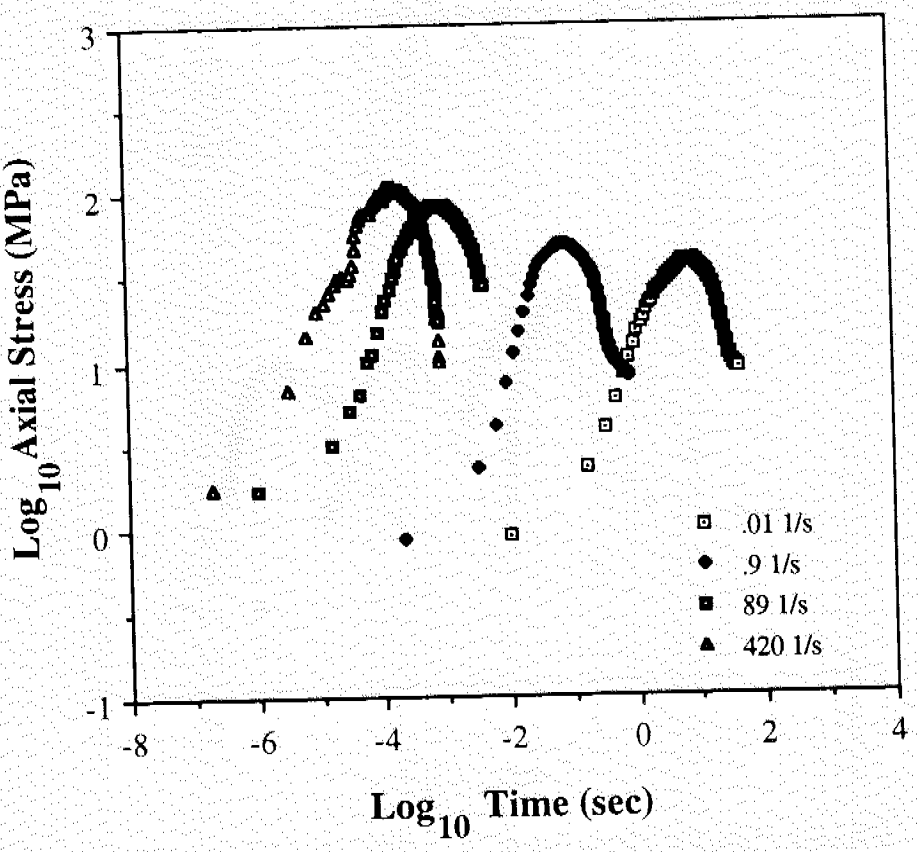

Figure 1. Axial Stress versus Time at Various Strain Rates in M30 Gun Propellant.

Table 1. Chemical Composition and Nominal Specimen Dimensions of M30 Gun Propellant

Component	%
Nitrocellulose	28.0
% NC Nitration	12.6
Nitroglycerin	22.0
Nitroguanidine	48.0
Ethyl Centralite	2.0
Length (mm)	25.4
Diameter (mm)	12.3

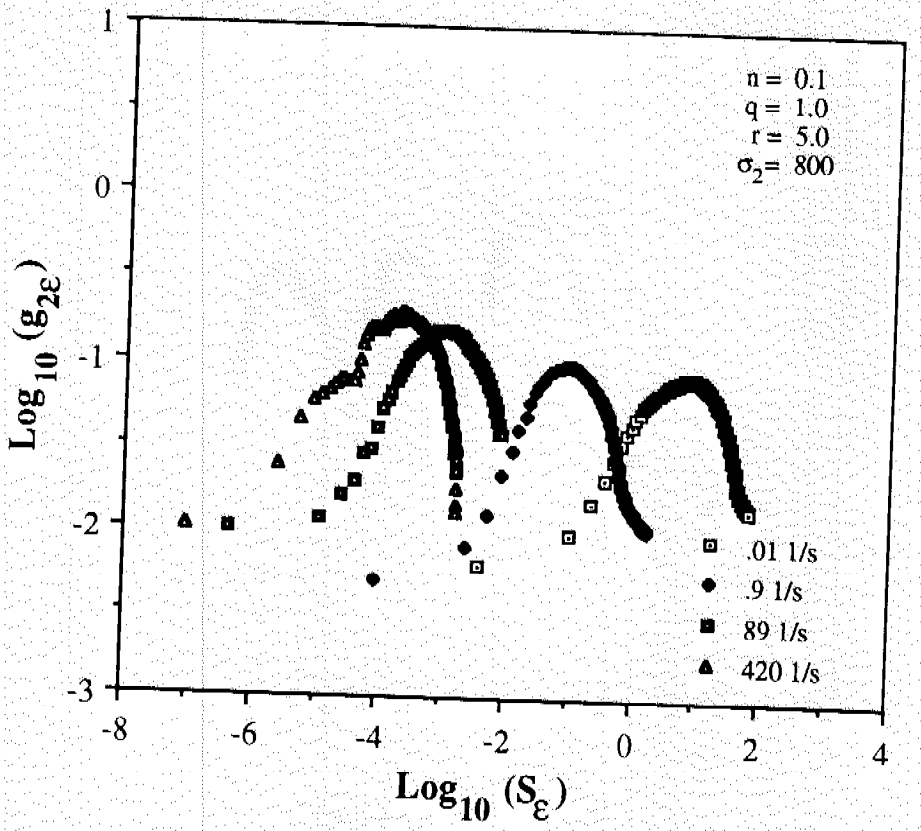

Figure 2. Damage Function versus Damage Parameter as a Function of Strain Rate for Arbitrary Material Constants.

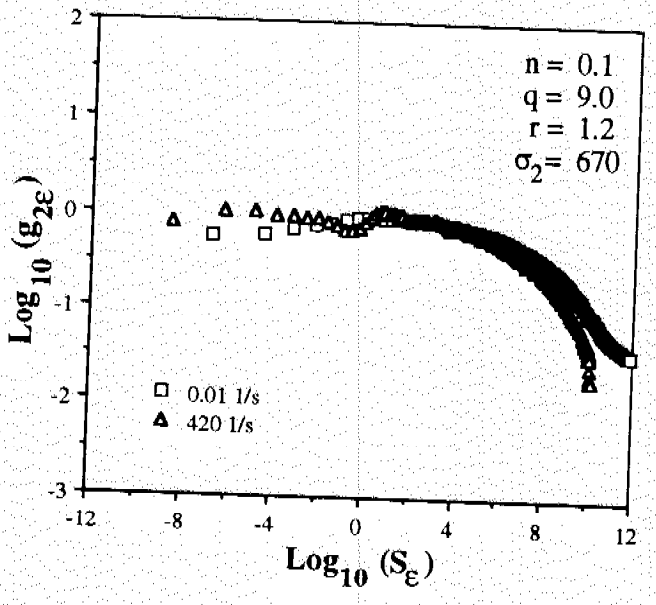

Figure 3a. "Master" Damage Function versus Damage Parameter Formed from Shifted Constant Strain Rate Test Data.

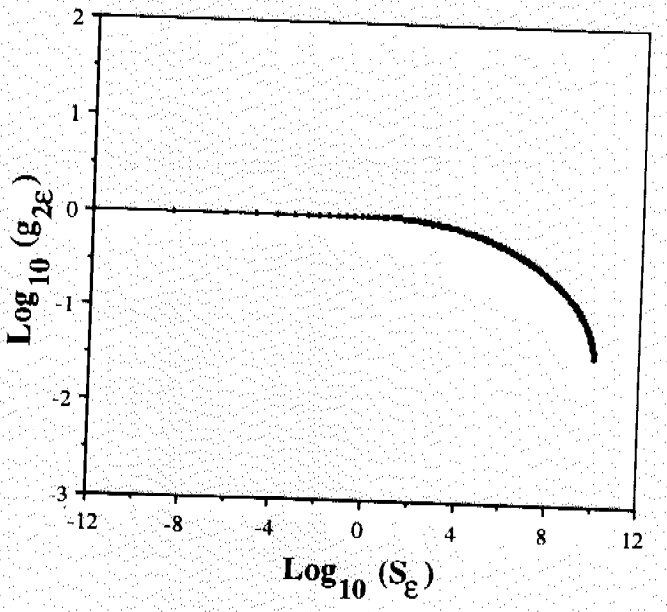

Figure 3b. "Ellipsoidal" Damage Function

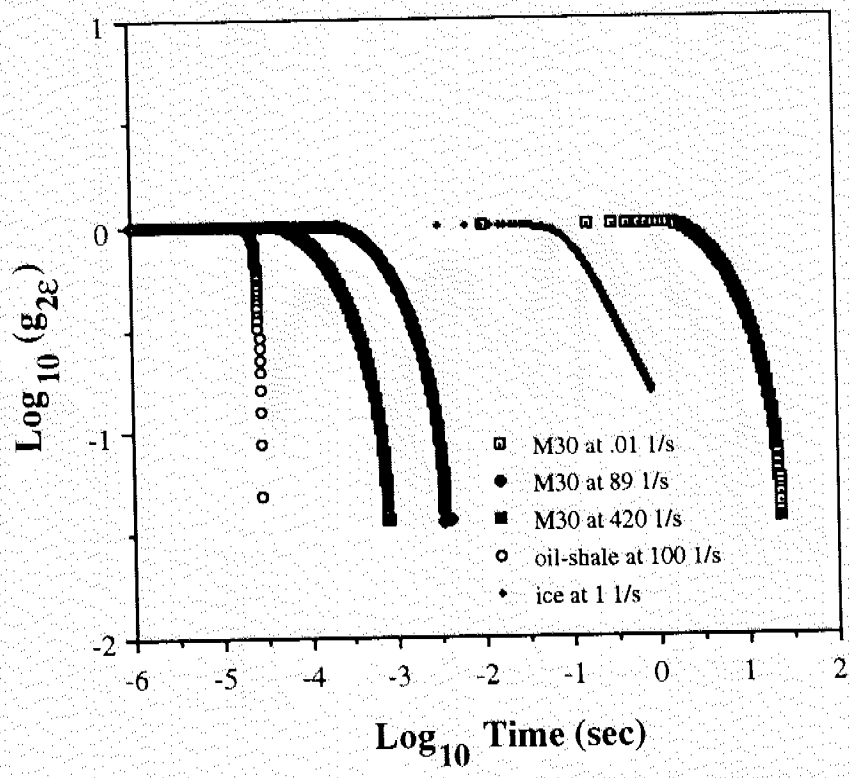

Figure 4a. Comparison of Damage Functions versus Time for M30 (symbols), Ice (+) (Harper 1986), and Oil Shale (o) (Grady and Kipp 1987).

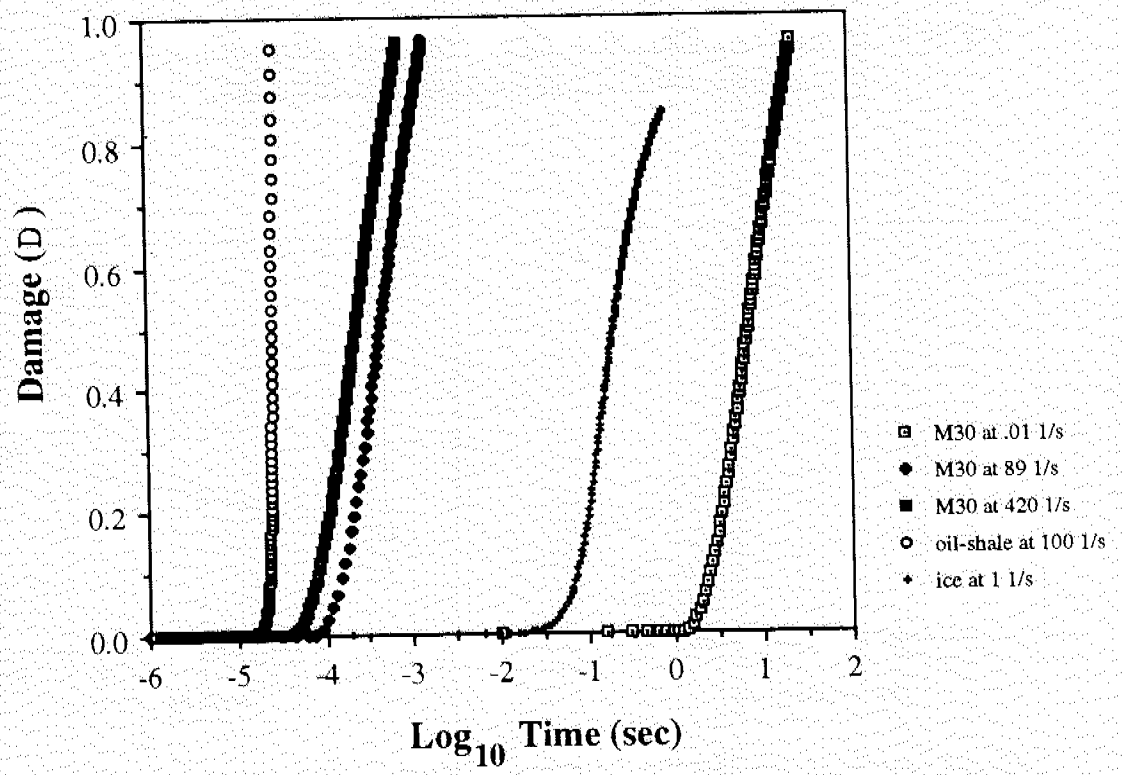

Figure 4b. Comparison of Damage versus Time for M30 (symbols), Ice (+) (Harper 1986), and Oil Shale (o) (Grady and Kipp 1987).

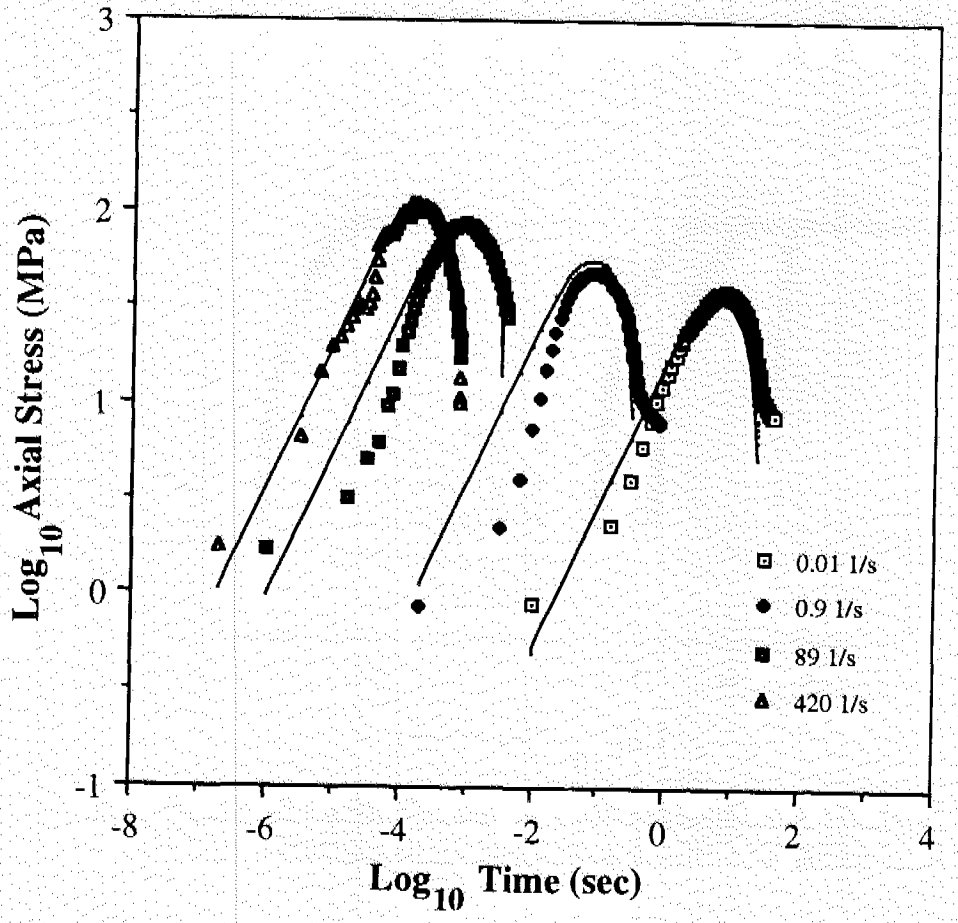

Figure 5. Overlay of Observed (symbols) and Theoretical (solid) Stress versus Time Curves for M30 Gun Propellant.

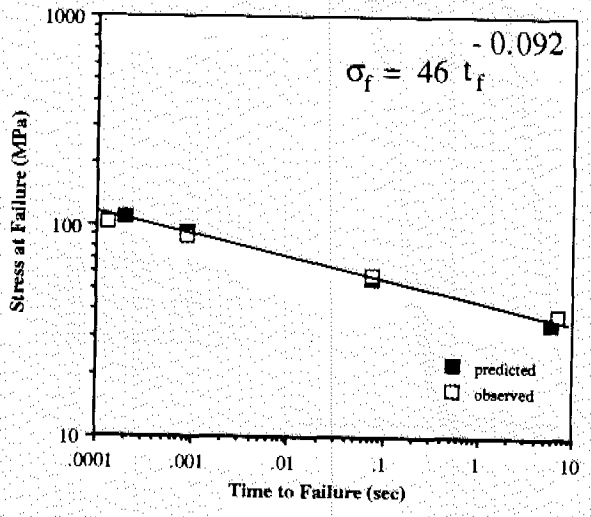

Figure 6. Stress at Failure versus Time to Failure.

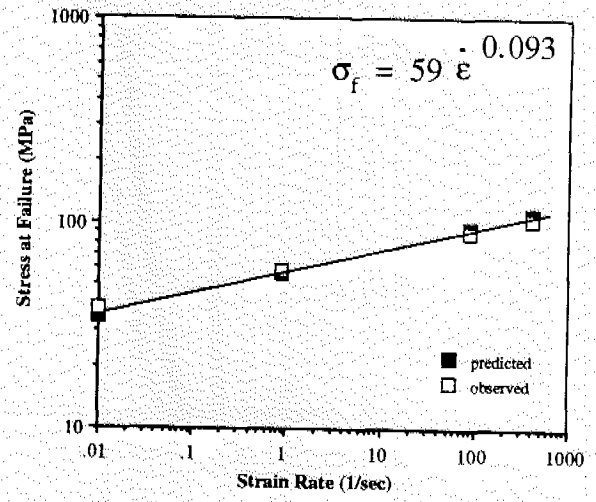

Figure 7. Stress at Failure versus Strain Rate.

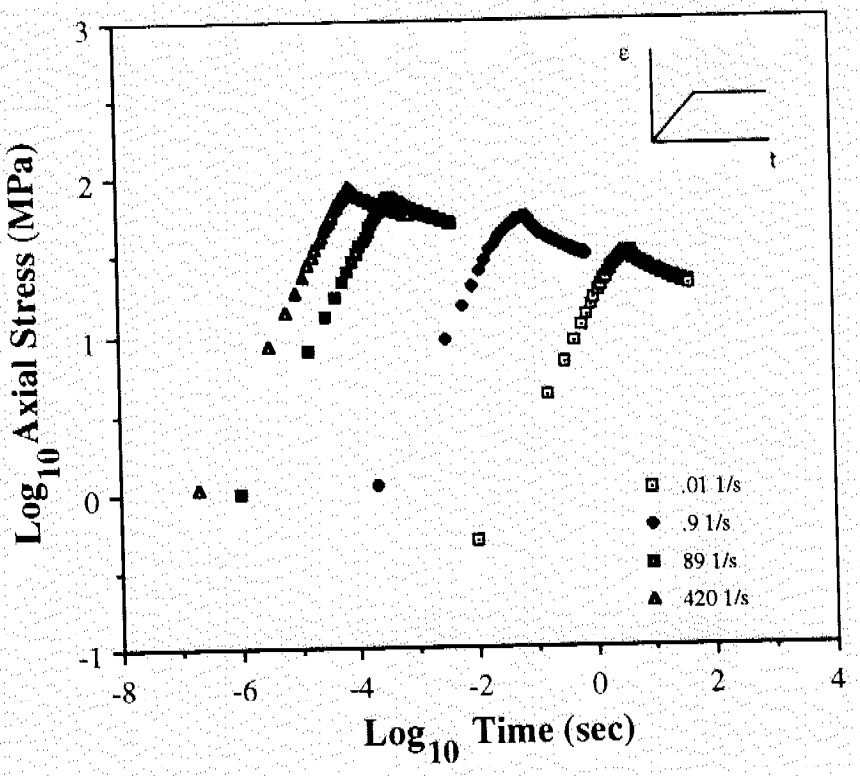

Figure 8. Predicted Stress versus Time for Two-Step Input History, Constant Strain Rate Followed by Constant Strain.

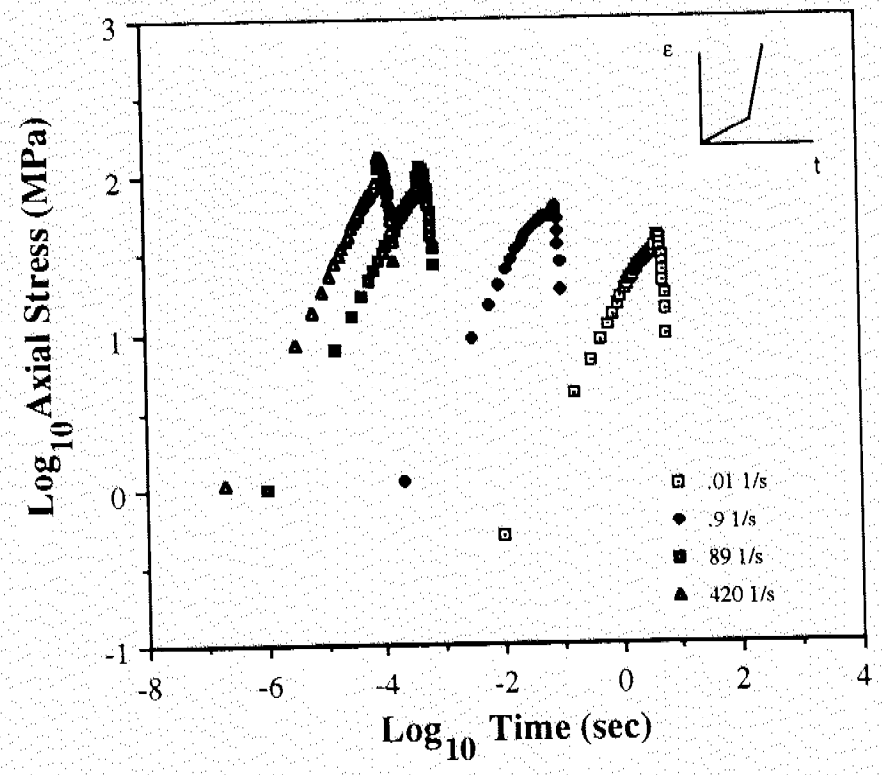

Figure 9. Predicted Stress versus Time for "Ballistic-Like" Input History, Constant Strain Rate Followed by Order-of-Magnitude Increase in Strain Rate.

INTENTIONALLY LEFT BLANK.

8. REFERENCES

Bolotin, V. V. Statistical Methods in Structural Mechanics, Edited by J. J. Brandstatter, Holden-Day, Inc., San Francisco, 1969.

Budiansky, B., and R.J. O'Connell. "Elastic Moduli of a Cracked Solid." Int. J. Solids Structures, Vol. 12, pp. 81-97, 1976.

Costin, L.S. "Time-Dependent Deformation and Failure." in: Fracture Mechanics of Rock, Edited by B.K. Atkinson, London, Academic Press, Inc., pp. 167- 215, 1987.

Gazonas, G.A. "The Mechanical Response of M30, XM39, and JA2 Propellants at Strain Rates from 10^{-2} to 250 sec^{-1}." BRL-TR-3181, U.S. Army Ballistic Research Laboratory, Aberdeen Proving Ground, MD, January, 1991.

Gazonas, G.A., A. Juhasz and J.C. Ford. "Strain Rate Insensitivity of Damage-Induced Surface Area in M30 and JA2 Gun Propellants." BRL-TR-3251, U.S. Army Ballistic Research Laboratory, Aberdeen Proving Ground, MD, August, 1991.

Gazonas, G.A. and J.C. Ford. "Uniaxial Compression Testing of M30 and JA2 Gun Propellants Using a Statistical Design Strategy." Experimental Mechanics, Vol. 32, pp. 154-162, 1992.

Gough, P.S. "The XNOVAKTC Code." BRL-CR-627, U.S. Army Ballistic Research Laboratory, Aberdeen Proving Ground, MD, February, 1990.

Grady, D.E., and M.E. Kipp. "Continuum Modelling of Explosive Fracture in Oil Shale." Int. J. Rock Mech. Min. Sci. & Geomech. Abstr., Vol. 17., pp. 147-157, 1980.

Harper, B.D. "A Uniaxial Nonlinear Viscoelastic Constitutive Relation for Ice." Journal of Energy Resources Technology, Vol. 108, pp. 156-160, June 1986.

Harper, B.D. "Some Implications of a Nonlinear Viscoelastic Constitutive Theory Regarding Interrelationships Between Creep and Strength Behavior of Ice at Failure." Journal of Offshore Mechanics and Arctic Engineering, Vol. 111, pp. 144-148, May 1989.

Keller, G.E., and A.W. Horst. "The Effects of Propellant Grain Fracture on the Interior Ballistics of Guns." BRL-MR-3766, U.S. Army Ballistic Research Laboratory, Aberdeen Proving Ground, MD, June, 1989.

Krajcinovic, D. "Micromechanical Basis of Phenomenological Models." Continuum Damage Mechanics: Theory and Applications, Edited by D. Krajcinovic and J. Lemaitre, Springer Verlag, pp. 195-206, 1987.

Lemaitre, J. "A Continuous Damage Mechanics Model for Ductile Fracture." J. Engng. Mater. Technol., Vol. 107, pp. 83-89, 1985.

Lieb, R.J. "The Mechanical Response of M30, JA2 and XM39 Gun Propellants to High Rate Deformation." BRL-TR-3023, U.S. Army Ballistic Research Laboratory, Aberdeen Proving Ground, MD, August, 1989.

Lieb, R.J., T.J. Fischer and H.J. Hoffman. "High Strain Rate Response of Gun Propellant Using the Hopkinson Split Bar." Presented at the JANNAF Joint S&MBS/CMCS Meeting, JPL, Pasadena, CA, November, 1989.

Military Explosives, Departments of the Army and the Air Force Technical Manual No. 9-1910, Technical Order No. 11A-1-34, U.S. Government Printing Office, Washington, D.C., April, 1955.

Rousselier, J. Proceedings of IUTAM Symposium on 30 Constitutive Relations and Ductile Fracture, Edited by S. Nemat Nasser, North Holland Publishing, Co., pp. 331-335, 1981.

Schapery, R.A. "On Viscoelastic Deformation and Failure Behavior of Composite Materials with Distributed Flaws." 1981 Advances in Aerospace Structures and Materials, ASME, AD-01, Edited by S.S. Wang, and W.L. Renton, New York, pp. 5-20, 1981.

Schapery, R.A. "Models for Damage Growth and Fracture in Nonlinear Viscoelastic Particulate Composites." Proceedings of the Ninth U.S. National Congress of Applied Mechanics, ASME, pp. 237-245, 1982.

Schapery, R.A., and M. Riggins. "Development of Cyclic Non-linear Viscoelastic Constitutive Equations for Marine Sediment." International Symposium on Numerical Models in Geomechanics, Edited by R. Dungar, G.N. Pande, and J.A. Studer, Zurich, pp.172-182, 1982.

Schapery, R.A. "Models for the Deformation of Viscoelastic Media with Distributed Damage and their Applicability to Ice." Proceedings of the IUTAM/IAHR Symposium on Ice/Structure Interaction, Memorial University of Newfoundland, St. John's, August 1989.

Valanis, K.C. "A Global Damage Theory and the Hyperbolicity of the Wave Equation." Journal of Applied Mechanics, Vol. 58, pp. 311-316, 1991.

Weitsman, Y. "A Continuum Damage Model for Viscoelastic Materials." Journal of Applied Mechanics, vol. 55, pp. 773-780, December 1988.

Wnuk, M.P., and R.D. Kriz. "CDM Model of Damage in Laminated Composites." International Journal of Fracture, vol. 28, pp. 121-128, 1985.

APPENDIX A:

DERIVATION OF GENERALIZED DAMAGE FUNCTION AND DAMAGE PARAMETER

INTENTIONALLY LEFT BLANK.

9. APPENDIX A: DERIVATION OF GENERALIZED DAMAGE FUNCTION AND DAMAGE PARAMETER

The derivation of the generalized damage function and parameter given by (11) and (12) in the main text begins by taking the first time derivative (dotted quantity) of the function f in (3),

$$\dot{f} = g_1 \dot{g}_2 + g_2 \dot{g}_1 \tag{A.1}$$

and collecting terms to obtain,

$$\frac{\dot{f}}{f} = \frac{\dot{g}_2}{g_2} + \frac{\dot{g}_1}{g_1} \tag{A.2}$$

Since $g_1 = g_1(\sigma)$ and $g_2 = g_2(S_\sigma)$, ordinary derivatives of these quantities are,

$$\dot{g}_1 = \frac{dg_1}{d\sigma}\frac{d\sigma}{dt} \tag{A.3}$$

and

$$\dot{g}_2 = \frac{dg_2}{dS_\sigma}\frac{dS_\sigma}{dt} \tag{A.4}$$

Substitution of (A.3) and (A.4) and the first time derivative of the damage parmeter S_σ given in (4) from the main text into (A.2) yields the following nonlinear ordinary differential equation in σ, of Bernoulli form,

$$\sigma\frac{\dot{f}}{f} = \frac{dg_2}{dS_\sigma}\frac{\sigma^{q+1}}{\sigma_1^q}\frac{f_1}{g_2} + \sigma\dot{r} \tag{A.5}$$

where, $f_1 = f_1(t)$. A change of variables in (A.5) using,

$$u = \left|\frac{\sigma}{\sigma_2}\right|^{-q} \quad , \tag{A.6}$$

and

$$\dot{u} = \frac{-q\,\sigma^{-(q+1)}\,\dot{\sigma}}{\sigma_2^{-q}} \quad , \tag{A.7}$$

results in the following linear ordinary differential equation,

$$\dot{u} + p(t)u = h(t) \quad , \tag{A.8}$$

where

$$p(t) = \frac{\dot{f}}{f}\frac{q}{r} \quad \text{and} \quad h(t) = \frac{q}{r}\left(\frac{\sigma_2}{\sigma_1}\right)^{q}\frac{dg_2}{dS_\sigma}\frac{f_1}{g_2} \quad . \tag{A.9}$$

An integrating factor $\rho(t)$ for (A.8) is obtained by letting,

$$P(t) = \int p(t)\,dt = \frac{q}{r}\int \frac{\dot{f}}{f}\,dt = \frac{q}{r}\ln|f| + c \quad , \tag{A.10}$$

hence

$$\rho(t) = \pm\, e^{P(t)} = \pm\, e^{c}\,|f|^{q/r} \quad . \tag{A.11}$$

For $c = 0$ in (A.11), a solution to (A.8) is obtained for u given by,

$$f^{q/r}\,u = \int f^{q/r}\left\{\frac{q}{r}\left(\frac{\sigma_2}{\sigma_1}\right)^{q}\frac{dg_2}{dS_\sigma}\frac{f_1}{g_2}\right\}dt + c_o \quad . \tag{A.12}$$

Substitution of (A.6) into (A.12), using the identity (10), $f = e^{\circ}$, from the main text, and letting $c_o = 1$, one arrives at the generalized damage function (11) and damage parameter (12).

No. of
Copies Organization

2 Administrator
Defense Technical Info Center
ATTN: DTIC-DDA
Cameron Station
Alexandria, VA 22304-6145

1 Commander
U.S. Army Materiel Command
ATTN: AMCAM
5001 Eisenhower Ave.
Alexandria, VA 22333-0001

1 Director
U.S. Army Research Laboratory
ATTN: AMSRL-OP-CI-AD,
Tech Publishing
2800 Powder Mill Rd.
Adelphi, MD 20783-1145

1 Director
U.S. Army Research Laboratory
ATTN: AMSRL-OP-CI-AD,
Records Management
2800 Powder Mill Rd.
Adelphi, MD 20783-1145

2 Commander
U.S. Army Armament Research,
Development, and Engineering Center
ATTN: SMCAR-IMI-I
Picatinny Arsenal, NJ 07806-5000

2 Commander
U.S. Army Armament Research,
Development, and Engineering Center
ATTN: SMCAR-TDC
Picatinny Arsenal, NJ 07806-5000

1 Director
Benet Weapons Laboratory
U.S. Army Armament Research,
Development, and Engineering Center
ATTN: SMCAR-CCB-TL
Watervliet, NY 12189-4050

(Unclass. only)1 Commander
U.S. Army Rock Island Arsenal
ATTN: SMCRI-IMC-RT/Technical Library
Rock Island, IL 61299-5000

1 Director
U.S. Army Aviation Research
and Technology Activity
ATTN: SAVRT-R (Library)
M/S 219-3
Ames Research Center
Moffett Field, CA 94035-1000

No. of
Copies Organization

1 Commander
U.S. Army Missile Command
ATTN: AMSMI-RD-CS-R (DOC)
Redstone Arsenal, AL 35898-5010

1 Commander
U.S. Army Tank-Automotive Command
ATTN: ASQNC-TAC-DIT (Technical
Information Center)
Warren, MI 48397-5000

1 Director
U.S. Army TRADOC Analysis Command
ATTN: ATRC-WSR
White Sands Missile Range, NM 88002-5502

1 Commandant
U.S. Army Field Artillery School
ATTN: ATSF-CSI
Ft. Sill, OK 73503-5000

(Class. only)1 Commandant
U.S. Army Infantry School
ATTN: ATSH-CD (Security Mgr.)
Fort Benning, GA 31905-5660

(Unclass. only)1 Commandant
U.S. Army Infantry School
ATTN: ATSH-CD-CSO-OR
Fort Benning, GA 31905-5660

1 WL/MNOI
Eglin AFB, FL 32542-5000

Aberdeen Proving Ground

2 Dir, USAMSAA
ATTN: AMXSY-D
AMXSY-MP, H. Cohen

1 Cdr, USATECOM
ATTN: AMSTE-TC

1 Dir, ERDEC
ATTN: SCBRD-RT

1 Cdr, CBDA
ATTN: AMSCB-CI

1 Dir, USARL
ATTN: AMSRL-SL-I

10 Dir, USARL
ATTN: AMSRL-OP-CI-B (Tech Lib)

No. of Copies	Organization
1	Chairman DOD Explosives Safety Board Room 856-C Hoffman Bldg. 1 2461 Eisenhower Avenue Alexandria, VA 22331-0600
1	Headquarters U.S. Army Materiel Command ATTN: AMCICP-AD, M. Fisette 5001 Eisenhower Ave. Alexandria, VA 22333-0001
1	U.S. Army Ballistic Missile Defense Systems Command Advanced Technology Center P.O. Box 1500 Huntsville, AL 35807-3801
1	Department of the Army Office of the Product Manager 155mm Howitzer, M109A6, Paladin ATTN: SFAE-AR-HIP-IP, Mr. R. De Kleine Picatinny Arsenal, NJ 07806-5000
3	Project Manager Advanced Field Artillery System ATTN: SFAE-ASM-AF-E LTC D. Ellis T. Kuriata J. Shields Picatinny Arsenal, NJ 07801-5000
1	Project Manager Advanced Field Artillery System ATTN: SFAE-ASM-AF-Q, W. Warren Picatinny Arsenal, NJ 07801-5000
2	Commander Production Base Modernization Agency U.S. Army Armament Research, Development, and Engineering Center ATTN: AMSMC-PBM, A. Siklosi AMSMC-PBM-E, L. Laibson Picatinny Arsenal, NJ 07806-5000
4	PEO-Armaments Project Manager Tank Main Armament System ATTN: AMCPM-TMA AMCPM-TMA-105 AMCPM-TMA-120 AMCPM-TMA-AS, H. Yuen Picatinny Arsenal, NJ 07806-5000
5	Commander U.S. Army Armament Research, Development, and Engineering Center ATTN: SMCAR-CCD, D. Spring SMCAR-CCH-V, C. Mandala E. Fennell SMCAR-CCH-T, L. Rosendorf SMCAR-CCS Picatinny Arsenal, NJ 07806-5000
19	Commander U.S. Army Armament Research, Development, and Engineering Center ATTN: SMCAR-AEE, J. Lannon SMCAR-AEE-B, A. Beardell D. Downs S. Einstein S. Westley S. Bernstein J. Rutkowski B. Brodman P. O'Reilly R. Cirincione A. Grabowsky P. Hui J. O'Reilly SMCAR-AEE-WW, M. Mezger J. Pinto D. Wiegand P. Lu C. Hu SMCAR-AES, S. Kaplowitz Picatinny Arsenal, NJ 07806-5000
1	Commander U.S. Army Armament Research, Development and Engineering Center ATTN: SMCAR-HFM, E. Barrieres Picatinny Arsenal, NJ 07806-5000

No. of Copies	Organization
9	Commander U.S. Army Armament Research, Development and Engineering Center ATTN: SMCAR-FSA-T, M. Salsbury SMCAR-FSA-F, LTC R. Riddle SMCAR-FSC, G. Ferdinand SMCAR-FS, T. Gora SMCAR-FS-DH, J. Feneck SMCAR-FSS-A, R. Kopman B. Machek L. Pinder SMCAR-FSN-N, K. Chung Picatinny Arsenal, NJ 07806-5000
3	Director Benet Weapons Laboratories ATTN: SMCAR-CCB-RA, G.P. O'Hara G.A. Pflegl SMCAR-CCB-S, F. Heiser Watervliet, NY 12189-4050
2	Commander U.S. Army Research Office ATTN: Technical Library D. Mann P.O. Box 12211 Research Triangle Park, NC 27709-2211
1	Commander, USACECOM R&D Technical Library ATTN: ASQNC-ELC-IS-L-R, Myer Center Fort Monmouth, NJ 07703-5301
1	Commander U.S. Army Harry Diamond Laboratory ATTN: SLCHD-TA-L 2800 Powder Mill Rd. Adelphi, MD 20783-1145
1	Commandant U.S. Army Aviation School ATTN: Aviation Agency Fort Rucker, AL 36360
1	Program Manager U.S. Tank-Automotive Command ATTN: AMCPM-ABMS, T. Dean Warren, MI 48092-2498

No. of Copies	Organization
1	Project Manager U.S. Tank-Automotive Command Fighting Vehicle Systems ATTN: SFAE-ASM-BV Warren, MI 48397-5000
1	Project Manager, Abrams Tank System ATTN: SFAE-ASM-AB Warren, MI 48397-5000
1	Director HQ, TRAC RPD ATTN: ATCD-MA Fort Monroe, VA 23651-5143
2	Director U.S. Army Materials Technology Laboratory ATTN: SLCMT-ATL (2 cps) Watertown, MA 02172-0001
1	Commander U.S. Army Belvoir Research and Development Center ATTN: STRBE-WC Fort Belvoir, VA 22060-5006
1	Director U.S. Army TRAC-Ft. Lee ATTN: ATRC-L, Mr. Cameron Fort Lee, VA 23801-6140
1	Commandant U.S. Army Command and General Staff College Fort Leavenworth, KS 66027
1	Commandant U.S. Army Special Warfare School ATTN: Rev and Trng Lit Div Fort Bragg, NC 28307
1	Commander Radford Army Ammunition Plant ATTN: SMCAR-QA/HI LIB Radford, VA 24141-0298

No. of
Copies Organization

1 Commander
U.S. Army Foreign Science and
Technology Center
ATTN: AMXST-MC-3
220 Seventh Street, NE
Charlottesville, VA 22901-5396

2 Commandant
U.S. Army Field Artillery
Center and School
ATTN: ATSF-CO-MW, E. Dublisky
ATSF-CN, P. Gross
Ft. Sill, OK 73503-5600

1 Commandant
U.S. Army Armor School
ATTN: ATZK-CD-MS, M. Falkovitch
Armor Agency
Fort Knox, KY 40121-5215

2 Commander
Naval Sea Systems Command
ATTN: SEA 62R
SEA 64
Washington, DC 20362-5101

1 Commander
Naval Air Systems Command
ATTN: AIR-954-Tech Library
Washington, DC 20360

4 Commander
Naval Research Laboratory
ATTN: Technical Library
Code 4410, K. Kailasanate
J. Boris
E. Oran
Washington, DC 20375-5000

1 Office of Naval Research
ATTN: Code 473, R.S. Miller
800 N. Quincy Street
Arlington, VA 22217-9999

1 Office of Naval Technology
ATTN: ONT-213, D. Siegel
800 N. Quincy St.
Arlington, VA 22217-5000

No. of
Copies Organization

4 Commander
Naval Surface Warfare Center
ATTN: Code 730
Code R-13,
R. Bernecker
H. Sandusky
Silver Spring, MD 20903-5000

7 Commander
Naval Surface Warfare Center
ATTN: T.C. Smith
K. Rice
S. Mitchell
S. Peters
J. Consaga
C. Gotzmer
Technical Library
Indian Head, MD 20640-5000

5 Commander
Naval Surface Warfare Center
ATTN: Code G30,
Code G32,
Code G33, J.L. East
T. Doran
Code E23 Technical Library
Dahlgren, VA 22448-5000

5 Commander
Naval Air Warfare Center
ATTN: Code 388, C.F. Price
T. Boggs
Code 3895, T. Parr
R. Derr
Information Science Division
China Lake, CA 93555-6001

2 Commanding Officer
Naval Underwater Systems Center
ATTN: Code 5B331, R.S. Lazar
Technical Library
Newport, RI 02840

1 AFOSR/NA
ATTN: J. Tishkoff
Bolling AFB, D.C. 20332-6448

1 OLAC PL/TSTL
ATTN: D. Shiplett
Edwards AFB, CA 93523-5000

No. of
Copies Organization

3 AL/LSCF
ATTN: J. Levine
L. Quinn
T. Edwards
Edwards AFB, CA 93523-5000

1 WL/MNAA
ATTN: B. Simpson
Eglin AFB, FL 32542-5434

1 WL/MNME
Energetic Materials Branch
2306 Perimeter Rd.
STE 9
Eglin AFB, FL 32542-5910

1 WL/MNSH
ATTN: R. Drabczuk
Eglin AFB, FL 32542-5434

2 NASA Langley Research Center
ATTN: M.S. 408, W. Scallion
D. Witcofski
Hampton, VA 23605

1 Central Intelligence Agency
Office of the Central References
Dissemination Branch
Room GE-47, HQS
Washington, DC 20502

1 Central Intelligence Agency
ATTN: J. Backofen
NHB, Room 5N01
Washington, DC 20505

1 SDIO/TNI
ATTN: L.H. Caveny
Pentagon
Washington, DC 20301-7100

1 SDIO/DA
ATTN: E. Gerry
Pentagon
Washington, DC 21301-7100

2 HQ DNA
ATTN: D. Lewis
A. Fahey
6801 Telegraph Rd.
Alexandria, VA 22310-3398

No. of
Copies Organization

1 Director
Sandia National Laboratories
Energetic Materials & Fluid Mechanics
Department, 1512
ATTN: M. Baer
P.O. Box 5800
Albuquerque, NM 87185

1 Director
Sandia National Laboratories
Combustion Research Facility
ATTN: R. Carling
Livermore, CA 94551-0469

4 Director
Lawrence Livermore National
Laboratory
ATTN: L-355,
A. Buckingham
G. Benedetti
M. Finger
L-324, M. Constantino
P.O. Box 808
Livermore, CA 94550-0622

2 Director
Los Alamos Scientific Lab
ATTN: T3/D. Butler
M. Division/B. Craig
P.O. Box 1663
Los Alamos, NM 87544

3 Battelle Columbus Laboratories
ATTN: TACTEC Library,
J.N. Huggins
V. Levin
505 King Avenue
Columbus, OH 43201-2693

1 Battelle PNL
ATTN: Mr. Mark Garnich
P.O. Box 999
Richland, WA 99352

1 Institute of Gas Technology
ATTN: D. Gidaspow
3424 S. State Street
Chicago, IL 60616-3896

No. of
Copies Organization

1 Institute for Advanced Technology
ATTN: T.M. Krehne
The University of Texas of Austin
4030-2 W. Braker Lane
Austin, TX 78759-5329

2 CPIA - JHU
ATTN: Hary J. Hoffman
T. Christian
10630 Little Patuxent Parkway
Suite 202
Columbia, MD 21044-3200

1 Brigham Young University
Department of Chemical Engineering
ATTN: M. Beckstead
Provo, UT 84601

1 Jet Propulsion Laboratory
California Institute of Technology
ATTN: L.D. Strand, MS 125/224
4800 Oak Grove Drive
Pasadena, CA 91109

1 California Institute of Technology
204 Karman Lab
Main Stop 301-46
ATTN: F.E.C. Culick
1201 E. California Street
Pasadena, CA 91109

3 Georgia Institute of Technology
School of Aerospace Engineering
ATTN: B.T. Zim
E. Price
W.C. Strahle
Atlanta, GA 30332

1 Massachusetts Institute of Technology
Department of Mechanical Engineering
ATTN: T. Toong
77 Massachusetts Avenue
Cambridge, MA 02139-4307

1 University of Illinois
Department of Mechanical/Industry
Engineering
ATTN: H. Krier
144 MEB; 1206 N. Green St.
Urbana, IL 61801-2978

No. of
Copies Organization

1 University of Maryland
ATTN: Dr. J.D. Anderson
College Park, MD 20740

1 University of Massachusetts
Department of Mechanical Engineering
ATTN: K. Jakus
Amherst, MA 01002-0014

1 University of Minnesota
Department of Mechanical Engineering
ATTN: E. Fletcher
Minneapolis, MN 55414-3368

3 Pennsylvania State University
Department of Mechanical Engineering
ATTN: V. Yang
K. Kuo
C. Merkle
University Park, PA 16802-7501

1 Rensselaer Polytechnic Institute
Department of Mathematics
Troy, NY 12181

1 Stevens Institute of Technology
Davidson Laboratory
ATTN: R. McAlevy III
Castle Point Station
Hoboken, NJ 07030-5907

1 Rutgers University
Department of Mechanical and
Aerospace Engineering
ATTN: S. Temkin
University Heights Campus
New Brunswick, NJ 08903

1 University of Southern California
Mechanical Engineering Department
ATTN: 0HE200, M. Gerstein
Los Angeles, CA 90089-5199

1 University of Utah
Department of Chemical Engineering
ATTN: A. Baer
Salt Lake City, UT 84112-1194

1 Washington State University
Department of Mechanical Engineering
ATTN: C.T. Crowe
Pullman, WA 99163-5201

No. of Copies	Organization
1	AFELM, The Rand Corporation ATTN: Library D 1700 Main Street Santa Monica, CA 90401-3297
1	Arrow Technology Associates, Inc. ATTN: W. Hathaway P.O. Box 4218 South Burlington, VT 05401-0042
3	AAI Corporation ATTN: J. Hebert J. Frankle D. Cleveland P.O. Box 126 Hunt Valley, MD 21030-0126
2	Alliant Techsystems, Inc. ATTN: R.E. Tompkins J. Kennedy 7225 Northland Dr. Brooklyn Park, MN 55428
1	AVCO Everett Research Laboratory ATTN: D. Stickler 2385 Revere Beach Parkway Everett, MA 02149-5936
1	General Applied Sciences Lab ATTN: J. Erdos 77 Raynor Ave. Ronkonkama, NY 11779-6649
1	General Electric Company Tactical System Department ATTN: J. Mandzy 100 Plastics Ave. Pittsfield, MA 01201-3698
1	IITRI ATTN: M.J. Klein 10 W. 35th Street Chicago, IL 60616-3799
5	Hercules, Inc. Radford Army Ammunition Plant ATTN: D.A. Worrell W.J. Worrell R. Goft C. Chandler L. Rivenbark Radford, VA 24141-0299
2	Hercules, Inc. Allegheny Ballistics Laboratory ATTN: William B. Walkup Thomas F. Farabaugh P.O. Box 210 Rocket Center, WV 26726
1	Hercules, Inc. Hercules Plaza ATTN: B.M. Riggleman Wilmington, DE 19894
1	MBR Research Inc. ATTN: Dr. Moshe Ben-Reuven 601 Ewing St., Suite C-22 Princeton, NJ 08540
1	Olin Corporation Badger Army Ammunition Plant ATTN: F.E. Wolf Baraboo, WI 53913
3	Olin Ordnance ATTN: E.J. Kirschke A.F. Gonzalez D.W. Worthington P.O. Box 222 St. Marks, FL 32355-0222
1	Olin Ordnance ATTN: H.A. McElroy 10101 9th Street, North St. Petersburg, FL 33716
1	Paul Gough Associates, Inc. ATTN: P.S. Gough 1048 South St. Portsmouth, NH 03801-5423
1	Physics International Library ATTN: H. Wayne Wampler P.O. Box 5010 San Leandro, CA 94577-0599
2	Princeton Combustion Research Laboratories, Inc. ATTN: N. Mer N.A. Messina Princeton Corporate Plaza 11 Deerpark Dr., Bldg IV, Suite 119 Monmouth Junction, NJ 08852

No. of
Copies Organization

3 Rockwell International
Rocketdyne Division
ATTN: BA08,
J. Flanagan
J. Gray
R.B. Edelman
6633 Canoga Avenue
Canoga Park, CA 91303-2703

2 Rockwell International Science Center
ATTN: Dr. S. Chakravarthy
Dr. S. Palaniswamy
1049 Camino Dos Rios
P.O. Box 1085
Thousand Oaks, CA 91360

1 Southwest Research Institute
ATTN: J.P. Riegel
6220 Culebra Road
P.O. Drawer 28510
San Antonio, TX 78228-0510

1 Sverdrup Technology, Inc.
ATTN: Dr. John Deur
2001 Aerospace Parkway
Brook Park, OH 44142

2 Thiokol Corporation
Elkton Division
ATTN: R. Biddle
Tech Library
P.O. Box 241
Elkton, MD 21921-0241

1 Veritay Technology, Inc.
ATTN: E. Fisher
4845 Millersport Hwy.
East Amherst, NY 14501-0305

1 Universal Propulsion Company
ATTN: H.J. McSpadden
25401 North Central Ave.
Phoenix, AZ 85027-7837

1 SRI International
Propulsion Sciences Division
ATTN: Tech Library
333 Ravenwood Avenue
Menlo Park, CA 94025-3493

No. of
Copies Organization

Aberdeen Proving Ground

1 Cdr, USACSTA
ATTN: STECS-PO/R. Hendricksen

No. of Copies	Organization
1	Ernst-Mach-Institut ATTN: Dr. R. Heiser Haupstrasse 18 Weil am Rheim Germany
1	Defence Research Agency, Military Division ATTN: C. Woodley RARDE Fort Halstead Sevenoaks, Kent, TN14 7BP England
1	School of Mechanical, Materials, and Civil Engineering ATTN: Dr. Bryan Lawton Royal Military College of Science Shrivenham, Swindon, Wiltshire, SN6 8LA England
2	Institut Saint Louis ATTN: Dr. Marc Giraud Dr. Gunther Sheets Postfach 1260 7858 Weail am Rhein 1 Germany
1	Explosive Ordnance Division ATTN: A. Wildegger-Gaissmaier Defence Science and Technology Organisation P.O. Box 1750 Salisbury, South Australia 5108
1	Armaments Division ATTN: Dr. J. Lavigne Defence Research Establishment Valcartier 2459, Pie XI Blvd., North P.O. Box 8800 Courcelette, Quebec G0A 1R0 Canada
1	U.S. Army European Research Office ATTN: Dr. Roy E. Richenbach Box 65 FPO New York 09510-1500

INTENTIONALLY LEFT BLANK.

USER EVALUATION SHEET/CHANGE OF ADDRESS

This Laboratory undertakes a continuing effort to improve the quality of the reports it publishes. Your comments/answers to the items/questions below will aid us in our efforts.

1. ARL Report Number ARL-TR-115 Date of Report April 1993

2. Date Report Received _____

3. Does this report satisfy a need? (Comment on purpose, related project, or other area of interest for which the report will be used.) _____

4. Specifically, how is the report being used? (Information source, design data, procedure, source of ideas, etc.) _____

5. Has the information in this report led to any quantitative savings as far as man-hours or dollars saved, operating costs avoided, or efficiencies achieved, etc? If so, please elaborate. _____

6. General Comments. What do you think should be changed to improve future reports? (Indicate changes to organization, technical content, format, etc.) _____

CURRENT ADDRESS

_____
Organization

_____
Name

_____
Street or P.O. Box No.

_____
City, State, Zip Code

7. If indicating a Change of Address or Address Correction, please provide the Current or Correct address above and the Old or Incorrect address below.

OLD ADDRESS

_____
Organization

_____
Name

_____
Street or P.O. Box No.

_____
City, State, Zip Code

(Remove this sheet, fold as indicated, tape closed, and mail.)
(DO NOT STAPLE)

DEPARTMENT OF THE ARMY

OFFICIAL BUSINESS

NO POSTAGE
NECESSARY
IF MAILED
IN THE
UNITED STATES

BUSINESS REPLY MAIL
FIRST CLASS PERMIT No 0001, APG, MD

Postage will be paid by addressee

Director
U.S. Army Research Laboratory
ATTN: AMSRL-OP-CI-B (Tech Lib)
Aberdeen Proving Ground, MD 21005-5066